

## Determination of the basic parameters of the high-frequency planar transformer

**Abstract.** The study is dedicated to the experimental and analytical determination of the parameters of the  $\pi$ -shape circuit models of high-frequency two-winding planar transformers used in various types of power electronic converters. For determining the winding capacitance, magnetizing and leakage inductances, waveforms of the voltage and current in the primary winding of a no-loaded and short-circuit transformer were used. The resistances of both windings for alternating current and the resistance corresponding to power losses in magnetic core were determined analytically based on Dowell's and Steinmetz's formulas, while considering the effect of temperature. The subject under consideration was a 5600 VA planar ferrite-core transformer designed for operating with a rectangular-wave primary voltage of 360 V and a frequency equal 100 kHz.

**Streszczenie.** Pracę poświęcono eksperymentalnemu i analitycznemu wyznaczaniu parametrów modeli obwodowych kształtu  $\pi$  wysokoczęstotliwościowych dwuuzwojeniowych transformatorów planarnych stosowanych w różnego rodzaju przekształtnikach energoelektronicznych. Do wyznaczania pojemności uzwojeń, indukcyjności magnesującej i indukcyjności rozproszenia wykorzystano oscylogramy napięcia i prądu uzwojenia pierwotnego transformatora pracującego bez obciążenia i w stanie zwarcia. Rezystancje obu uzwojeń dla prądu przemiennego oraz rezystancję odpowiadającą stratom mocy w rdzeniu wyznaczono analitycznie na podstawie wzorów Dowell'a i Steinmetz'a, uwzględniając przy tym wpływ temperatury. Przedmiotem rozważań był transformator z planarnym rdzeniem ferrytowym o mocy 5600 VA przeznaczony do pracy przy prostokątnym napięciu pierwotnym 360 V i częstotliwości 100 kHz. (**Wyznaczenie podstawowych parametrów modelu obwodowego wysokoczęstotliwościowego transformatora planarnego.**)

**Keywords:** high-frequency planar transformer, transformer circuit model, stray capacitance and leakage inductance, transformer electrothermal model.

**Słowa kluczowe:** transformator wysokoczęstotliwościowy, model obwodowy transformatora, pojemność i indukcyjność rozproszenia, model elektrotermiczny transformatora.

### Introduction

High-frequency (above 20 kHz) transformers are basic components of a numerous group of power electronic converters that include switch mode power supplies and different types of uni- or a bidirectional DC/DC circuit coupling systems, which ensure galvanic separation and voltage matching (e.g. [1], [2], [3]). Planar transformers are gaining particular importance, which, owing to their high energy efficiency and, at the same time, simple construction enable converters of a unit power of up to several kilowatts and a power density of about 10 kW/dm<sup>3</sup> to be constructed. They find increasingly wide application in electric power engineering, e.g. in systems for bidirectional energy transmission between energy storages and a smart-grid type network with renewable energy sources [4], [5]. They are also used for building intelligent converter transformers or even direct current high-voltage electric energy transmission systems (HVDC) [6].

Transformer electric parameters, including those of a parasitic nature, not only determine the correct operation of the transformer itself, but also influence the operation conditions of elements directly connected with the transformer's windings, as well as the properties of the whole power electronic unit.

In the case of high-frequency transformers, the effect of parameters referred to as parasitic, including primarily the stray capacitance, and in some cases also leakage inductance, becomes especially noticeable. In transistor hard-switching converters, the resonance phenomena caused by those parameters may result in an increase in power losses in semiconductor switches and the occurrence of dangerous overvoltages on them. Transformer parasitic capacitances are the cause of high-frequency oscillatory deformations of the transformer's voltages and currents, resulting in added power losses in the transformer and reducing the energy efficiency of the whole unit (Fig. 1).

The undesired resonance phenomena increase the level of electromagnetic disturbances. It is also clear that parameters, such as the winding resistance and the

resistance corresponding to the transformer core power losses, significantly contribute to a reduction of converter efficiency [7].

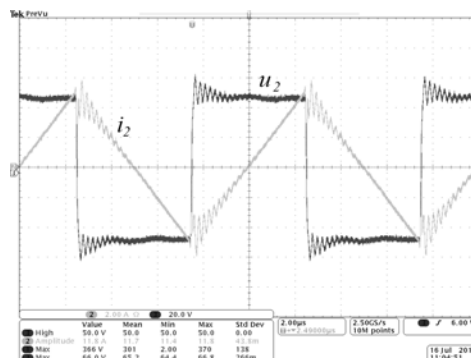


Fig. 1. Example waveforms of a high-frequency transformer's winding voltage  $u_2$  and current  $i_2$  with distinct oscillations caused by parasitic winding parameters (power supply from the low-voltage side; 20 V/div.; 2 A/div.; 2  $\mu$ s/div)

In some instances, transformer dissipation capacitance and inductance are used as quantities being an integral part of circuits operating directly with the transformer or other magnetic element. This applies to, e.g., resonance converters, in which a semiconductor component soft-switching technique is employed [7]-[13]. The transformer leakage inductance, which increases the resultant inductance of the alternating current circuit of DC/DC converters with a double active bridge (DAB) topology, is used for shaping the characteristics of the control of energy transfer between coupled direct current circuits [5].

Transformer electric parameters depend on many factors, such as geometric dimensions, the properties of materials used, the shape and spatial arrangement of the windings and the performance of their sections and layers. Hence, both the analytical and simulation determination of these parameters is complex.

Relatively accurate values of the parameters of the transformer circuit model are often obtained by using numerical methods, such as the finite element method (FEM). Such numerical modelling is, however, very time-consuming and requires a good knowledge of the software. This being especially true for planar transformers (e.g. [2], [3], [14], [15]). But even advanced software will not always guarantee the satisfactory accuracy. For instance, study [2] compared the results of numerical computations (by the FEM method) with the results of experimental measurements of the leakage inductance of a ferrite-core transformer. The theoretical results turned out to be two times smaller than the experimental results, which indicates, above all, the imperfection of the theoretical approach with respect to this particular parameter. Also measurements using impedance analyzers, due to low levels of measurement signals, are little accurate [16]. Therefore, measurements with voltages and currents similar or identical to those occurring during transformer operation, should be regarded as the most reliable.

The majority of publications reporting the experimental studies of high-frequency transformers are devoted primarily to power losses released in the windings and the core (e.g. [2], [3], [17] - [19]), corresponding to which in circuits models are winding resistances for alternating current and resistances connected in parallel to the magnetizing inductance. Among publications concerned with other parameters of the high-frequency transformer circuit model, studies [20], [21] are worth noting, which report an experimental method of determining the transformer parasitic capacitance (stray capacitance), but for a transformer with cylindrical rather than planar windings.

This paper presents the experimental determination of the parasitic capacitance, leakage inductance and magnetizing inductance, which constitute the basic parameters of the 5600 VA/100 kHz  $\pi$ -shape planar transformer circuit model. Analytical relationships are also provided, which utilize Dowell's and Steinmetz's formulas, based on which the remaining transformer model parameters have been determined, namely the winding resistances for alternating current and the resistance corresponding to the planar ferrite-core power losses with rectangular-wave voltage. It has been assumed that the stray capacitance is concentrated and occurs on the primary (high-voltage) side of the transformer. A model of this type is very useful for the analysis and simulation study of complete DC/DC or another converters.

An IGBT transistor H-bridge voltage fed inverter was used in the experimental tests. Section 2 provides relationships describing the parameters of the high-frequency transformer model, in which concentrated parasitic capacitance occurs, among others. Section 3 is devoted to the description of the construction of a planar transformer selected to illustrate the proposed method of determining the circuit model parameters. Section 4 reports the results of experimental studies and the results of analytical calculations of the parameters of the model under consideration. A summary and conclusions are given in Section 5.

### High-Frequency Transformer Models

The double-winding high-frequency transformer circuit model shown in Fig. 2 includes elements representing the leakage inductances,  $L_{\sigma 1}$  and  $L_{\sigma 2}$ , respectively, for the primary (high-voltage) and the secondary (low-voltage) winding; the resistances,  $R_{\sigma 1}$  and  $R_{\sigma 2}$ , of the primary and secondary windings for alternating current of a specific frequency; the self-capacitances,  $C_{\sigma 10}$  and  $C_{\sigma 20}$ , of the

windings; and the mutual capacitance,  $C_{\sigma 120}$ , between the windings. In addition to the above-mentioned components, the equivalent circuit diagram contains also the resistance  $R_{Fe}$  corresponding to the core power losses, the magnetizing inductance  $L_m$ , on which the the induced voltage  $N_1 d\phi/dt = L_m di_{Lm}/dt$  occurs (where:  $\phi$  – main flux in the core,  $i_{Lm}$  – magnetizing current,  $N_1$  – number of primary winding turns), and the ideal transformer  $T_{ri}$ , represented by the voltage ratio  $n = N_2/N_1$ .

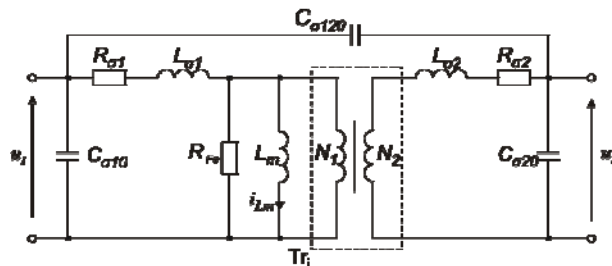


Fig. 2. The high-frequency double-winding transformer circuit model

Figure 3 shows the equivalent circuit diagram resulting from the transformation of the circuit model from Fig. 2 (e.g. [3], [7], [21]-[23]). The transformation consists in bringing all secondary circuit parameters to the primary side of the transformer, according to the following relationships:

- (1)  $u_2' = \frac{u_2}{n}$
- (2)  $i_2' = i_2 n$
- (3)  $R_{\sigma 2}' = \frac{R_{\sigma 2}}{n^2}$
- (4)  $L_{\sigma 2}' = \frac{L_{\sigma 2}}{n^2}$
- (5)  $C_{\sigma 1} = C_{\sigma 10} + (1-n)C_{\sigma 120}$
- (6)  $C_{\sigma 2}' = n^2 C_{\sigma 20} + n(n-1)C_{\sigma 120}$
- (7)  $C_{\sigma 12} = n C_{\sigma 120}$

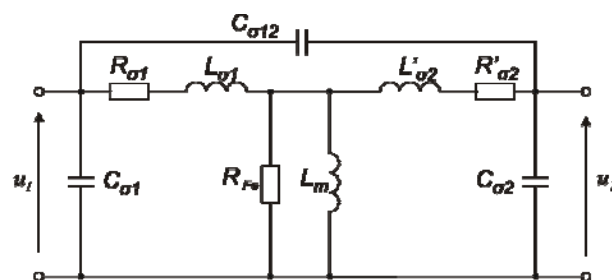


Fig. 3. The equivalent circuit diagram of a transformer with the parameters brought to the primary side

The leakage inductances  $L_{\sigma 1}$  and  $L_{\sigma 2}'$  of high-frequency planar transformers are smaller than 1% of the magnetizing inductance  $L_m$ . Hence, voltage drops caused by leakage inductances are negligible enough to allow the three dissipation capacitances  $C_{\sigma 12}$ ,  $C_{\sigma 1}$  and  $C_{\sigma 2}'$  to be substituted

with one lumped capacitance resulting from the parallel connection of  $C_{\sigma 1}$  and  $C_{\sigma 2}$  (Fig.4) [3].

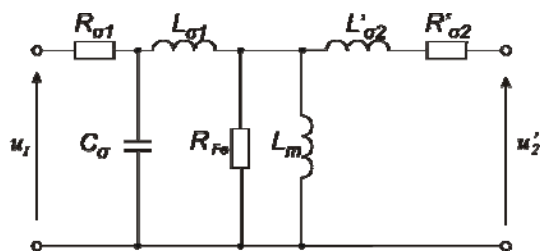


Fig. 4. The equivalent circuit diagram of a transformer with one lumped parasitic capacitance

#### Equivalent circuit diagram of an unloaded transformer

Planar transformers are distinguished by relatively high energy efficiency, exceeding even 99%. So, when analyzing a transformer operating without loading, the winding resistances can be omitted [21]. Figure 5 shows a simplified circuit diagram of a high-frequency transformer, which can be used for determining the parasitic capacitance and the magnetizing inductance [7], [21].

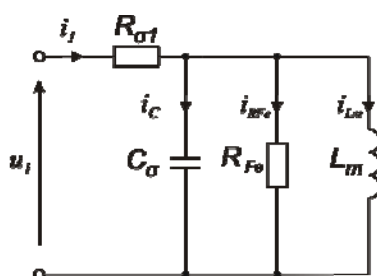


Fig. 5. Equivalent circuit diagram of an unloaded transformer

Due to a large value of magnetizing inductance compared to those of leakage inductances it can be assumed that the magnetizing current  $i_{Lm}$  with rectangular-wave supply voltage  $u_1$  has a triangular waveform (Fig. 6).

During the changes of voltage  $u_1$  polarization, i.e. in the intervals  $t_1 - t_2$   $t_3 - t_4$  part of the current  $i_{Lm}$  is the result of the discharging of the parasitic capacitance. In the interval  $t_1 - t_2$  the following relationships apply

$$(9) \quad i_{C\sigma} = i_1 - i_{Lm} - i_{RFe}$$

$$(10) \quad u_{C\sigma} = -U_m + \frac{1}{C_{\sigma}} \int_{t_1}^{t_2} i_{C\sigma} dt$$

Assuming that in the interval  $t_1 - t_2$  an overcharging of the dissipation capacitance by  $2U_m$  occurs, then based on Eq. (10), the following is obtained

$$(11) \quad 2U_m = \frac{1}{C_{\sigma}} Q_{12}$$

while:  $Q_{12}$  – charge stored in the parasitic capacitance.

The waveform of the actual value of the current  $i_{C\sigma}$  has, in approximation, the shape of the triangle, whose surface area is equal to the charge  $Q_{12}$ . Hence

$$(12) \quad Q_{12} = \frac{1}{2} I_{Cm} (t_2 - t_1)$$

and

$$(13) \quad C_{\sigma} = \frac{Q_{12}}{2U_m} = \frac{1}{4U_m} I_{Cm} \Delta t_{12}$$

Assuming that the current  $i_{RFe}$  is negligibly small, the peak value of the current flowing through the dissipation capacitances  $I_{Cm}$  and the time  $\Delta t_{12} = t_2 - t_1$  can be determined based on the current  $i_1$  that is easy to observe by oscilloscope.

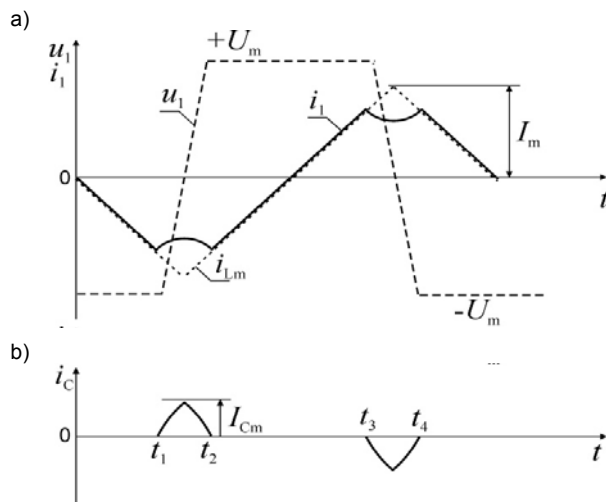


Fig. 6. Simplified waveforms of the actual values of primary winding voltage and current (a) and the current flowing through the parasitic capacitance of the transformer (b)

The equivalent circuit diagram in Fig. 5 can also be used for determining the magnetizing inductance. Based on this rectangular waveform of the voltage  $u_1$  with the period  $T$  and the triangular waveform of the current  $i_{Lm}$ , the following is obtained

$$(14) \quad L_m = \frac{T}{4I_m} U_m$$

where  $I_m$  is the peak value of the current  $i_{Lm}$  (Fig. 6).

In the case, where the catalogue core parameter  $A_L$ , which denotes the inductance of a single turn, is known, the value of the inductance  $L_m$  can be verified using the relationship:

$$(15) \quad L_m = A_L N_1^2$$

The experimental determination of the resistance  $R_{Fe}$  with the supply with rectangular-wave voltage is very difficult (e.g. [3], [17], [18]). In that case, it is recommended to use modified Steinmetz's formula, which enables the calculation of the power losses dissipated in the core. This formula, with rectangular-wave supply voltage, has the following form [18]

$$(16) \quad P_{Fe} = \frac{8}{\pi^2} k f^{\alpha} B_m^{\beta} (c_0 - c_1 T_T + c_2 T_T^2) V_{Fe}$$

while:  $f$  – inductance variation frequency [Hz],  $B_m$  – inductance waveform peak value [T],  $T_T$  – core temperature [°C],  $V_{Fe}$  – core volume [cm<sup>3</sup>].

To use formula (16), the coefficients of Steinmetz's equation ( $k$ ,  $\alpha$ ,  $\beta$ ) and the coefficients of the polynomial allowing for the temperature effect ( $c_0$ ,  $c_1$ ,  $c_2$ ) must be known. These coefficients are provided by core manufacturers.

The maximum value of induction, which with rectangular-wave of the voltage has a triangular waveform, can be determined from the relationship:

$$(17) \quad B_m = \frac{T}{4} \frac{1}{N_1 S_{Fe}} U_m$$

where:  $S_{Fe}$  – surface area of the core cross-section.

With the known power losses  $P_{Fe}$ , the resistance reflecting these power losses can be determined from the relationship:

$$(18) \quad R_{Fe} = \frac{U_m^2}{P_{Fe}}$$

In practice, the voltage  $U_m$  often changes. This is the case, e.g., in DAB systems coupling two direct voltage circuits, which usually exhibit large fluctuations [5].

The equivalent circuit diagram of a transformer in a short-circuit state

The resultant leakage inductance of the transformer

$$(19) \quad L_\sigma = L_{\sigma 1} + \frac{L_{\sigma 2}}{n^2}$$

can be determined by performing a short-circuit test. The equivalent circuit diagram of a transformer in a short-circuit state is shown in Fig. 7

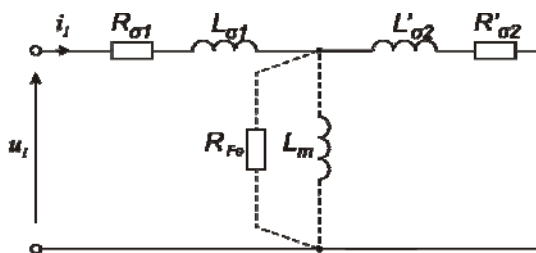


Fig. 7. The equivalent circuit diagram of a transformer in a short-circuit state

On account of the small short-circuit voltage values, amounting to merely a few percent of the rated voltage, the parameters  $R_{Fe}$ ,  $L_m$  and  $C_\sigma$  can be omitted in the equivalent circuit diagram of the transformer.

The circuit modelling the transformer in the short-circuit state is inductive in character, which means that with rectangular-wave supply voltage the winding current waveforms have an approximately triangular shape.

The resultant leakage inductance can be determined from the formula:

$$(20) \quad L_\sigma \approx \frac{T}{4 I_m} U_m$$

where:  $I_m$  is the peak value of the transformer's primary side current.

If in simulation studies, which use the transformer circuit model, there is the need for separating the resultant leakage inductance into the inductances  $L_{\sigma 1}$  and  $L_{\sigma 2}$ , it is usually assumed that  $L_{\sigma 1} = L'_{\sigma 2} = L_\sigma / 2$ .

Determining the alternating current winding resistances  $R_{\sigma 1}$  and  $R_{\sigma 2}$  based on experimental measurements is complex and involves the determination of the power

losses, whereas, the most accurate results are obtained via time-consuming thermal measurements (e.g. [18]).

Finding approximate winding resistance values is possible using Dowell's formulas [2], [3], [24]. With high voltage and current frequencies, as a result of the skin effect and the proximity effect, an increase in winding resistances will occur. In high-frequency planar transformers, the reduction of these phenomena is achieved primarily by using windings made from thin-gauge sheet metal, printed boards or litz wires, and by dividing the windings into sections and alternately positioning the primary and secondary windings.

The resistance of the  $j$ -th winding section composed of  $m_s$  layers can be expressed by formula [3], [24]

$$(21) \quad R_{ac(j)} = R_{d(j)} y \left[ \frac{\sinh(2y) + \sin(2y)}{\cosh(2y) - \cos(2y)} + \frac{2}{3} (m_s^2 - 1) \frac{\sinh(y) - \sin(y)}{\cosh(y) + \cos(y)} \right] = K_{R(j)} R_{d(j)}$$

where:  $R_{d(j)}$  – resistance of the  $j$ -th direct current winding section;  $K_{R(j)}$  – resistance increase coefficient of the  $j$ -th section with the flow of sinusoidal alternating current with the frequency  $f = 1/T$ ;  $m_s$  – number of layers in the  $j$ -th winding section;  $y$  – layer thickness relative to the skin depth, which, for copper winding at a frequency of 100 kHz and temperature of 20 °C is 0.227 mm.

When determining the resistances  $R_{\sigma 1}$  and  $R_{\sigma 2}$  for alternating current, it is necessary to define the resistance increase coefficients  $K_{R(j)}$  for individual sections, calculate the resistances of turns belonging to those sections,  $R_{\sigma(j)} = K_{R(j)} R_{d(j)}$ , and calculate the resultant winding resistances, while considering the series and parallel connections of the sections.

### Experimental Study of The Planar Transformer

Tests aimed at determining the transformer circuit model were carried out on a commercially available 5600 VA/100 kHz double-winding planar transformer with an ER 64/135/51 type ferrite core. The basic design specification of the transformer are given in Table 1.

Table 1. Specification of the transformer

Parameters	Values
Power	5600 VA
Operating frequency	100 kHz
Primary voltage (rectangular)	360 V
Turns ratio ( $N_2/N_1$ )	11/2
Thickness of PCB (primary windings)	0.05 mm (two parallel)
Thickness of cooper foil (secondary windings)	0.5 mm (two parallel)
Core type	ER 64/13/51
Core material	Ferrite 3F3
Core cross-section	566 mm <sup>2</sup>
Core volume	52.6 cm <sup>3</sup>

Figure 8 shows the transformer window cross-section with the windings and the winding connection arrangement. To reduce the proximity effect, the primary windings  $N_1$  and the secondary windings  $N_2$  have been divided into sections and positioned alternately (e.g. [3], [15], [23]).

Both windings are characterized by a large value of the ratio of conductor cross-section perimeter to conductor thickness, which is the necessary condition for the reduction

of eddy currents in the windings and the resulting increase in winding resistances at high current frequencies.

The primary windings are made from two multi-layered printed boards making up the sections  $s_2$  and  $s_4$ . They are connected in parallel, with each of them having 11 turns. When calculating the resistance  $R_{\sigma 1}$  of this winding, the number of layers  $m_{s_2} = m_{s_4} = 5.5$  should be assumed for each section.

The low-voltage winding is made from two copper sheets connected in parallel. This winding has two sections,  $s_1$  and  $s_5$ , each of them being composed of two layers ( $m_{s_1} = m_{s_5} = 2$ ), and one section,  $s_3$ , consisting of four layers, whereas, for the calculation of the resistance  $R_{\sigma 2}$  the number of layers  $m_{s_3} = 3$  should be taken.

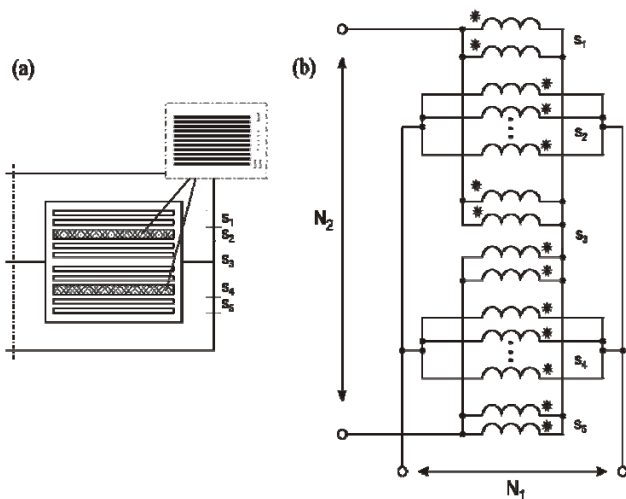


Fig. 8. The transformed winding: a) window cross-section; b) winding connection arrangement

### Circuit Model Parameters

#### Methodology

The parasitic (stray) capacitance  $C_{\sigma}$ , the magnetizing inductance  $L_m$  and the leakage inductance  $L_{\sigma}$  of the transformer were calculated by an experimental method involving the observation of primary winding voltage and current waveforms. The transformer was powered from a bridge voltage inverter consisting of four STW55NM60N type MOSFET silicon transistors (650V,  $r_{ON} = 47\text{m}\Omega$ ). The control pulses had a pulse-width modulation of 0.5, so that the inverter output voltage had a rectangular waveform with a frequency of  $f = 100$  kHz. The value of this voltage was controlled by changing the dc voltage at the inverter's input terminals. The dc voltage, depending on the type of the conducted tests and measured parameter, was varied in the range from 0 to 365 V. The observation of the waveforms was done using a DPO4034B type Tektronix oscilloscope with a voltage and current probe featuring a CWT Ultra Mini Rogowski coil manufactured by PEMUK.

The resistance  $R_{Fe}$  representing the core power losses and the winding resistance  $R_{\sigma 1}$  i  $R_{\sigma 2}$  were determined analytically from formulas (16) and (21) resulting from Steinmetz's and Dowell's models.

#### Parasitic capacitance and magnetizing inductance

The parasitic capacitance was determined based on the primary winding current  $i_1$  of the unloaded transformer (Fig. 9), read out from the primary winding voltage and current waveforms.

Oscilloscope measurements were taken at different inverter supply voltages  $E$ , varied in the range from 100 V to

365 V. In view of the large values of the voltages relative to the slight drops at the inverter's semiconductor switches, the positive and negative levels of winding voltage  $u_1$  can be regarded as constant, despite the fact that, in each of the semiconductor switches, the anti-parallel diode and then the transistor conducts in a given half-period.

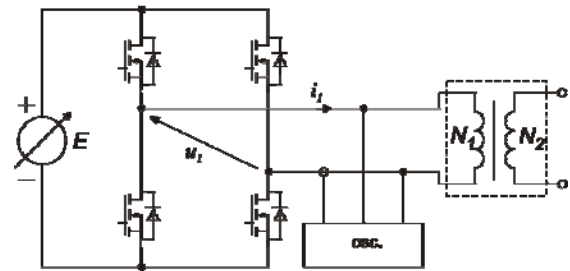


Fig. 9. A schematic diagram of the system for testing the unloaded transformer

Figure 10 shows an example of a primary winding voltage and current waveforms. After approximating the waveform of this current and determining the theoretical, unmeasurable capacitor current waveform according to Fig. 6b, the concentrated parasitic capacitance  $C_{\sigma}$  was calculated. This capacitance, for each recorded oscillogram, was calculated using formula (13). The measurement and calculation results for several voltages  $u_1$  are summarized in Table 2, while giving also the average value of capacitance  $C_{\sigma(AV)}$ .

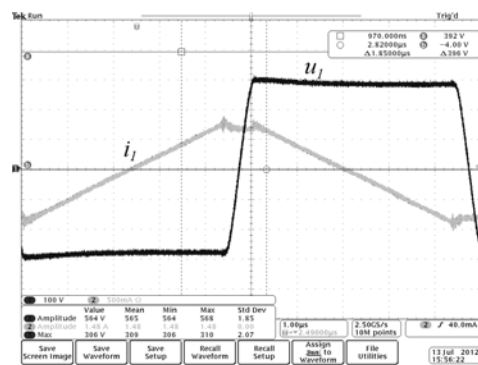


Fig. 10. The primary winding voltage  $u_1$  and current  $i_1$  waveforms for the unloaded transformer (100 V/div; 500 mA/div; 1 μs/div)

Table 2. Measurements and calculations of the parasitic capacitance

$U_m$ V	$I_{Cm}$ mA	$\Delta t$ $\mu\text{s}$	$C_{\sigma}$ nF	$C_{\sigma(AV)}$ nF
120	80	0.82	0.137	0.124
200	140	0.68	0.120	
284	220	0.66	0.130	
363	250	0.64	0.110	

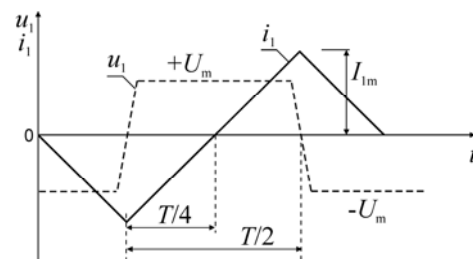


Fig. 11. Simplified waveforms of the primary winding voltage and current of the unloaded transformer

Table 3. Measurements and calculations of the magnetizing inductance

$U_m$	$I_{Im}$	$L_m$	$L_{m(AV)}$
V	A	$\mu\text{H}$	$\mu\text{H}$
120	0.42	720	770
200	0.625	800	
280	1.70	814	
360	1.20	753	

The waveforms of the current  $i_1$  and the voltage  $u_1$  at the unloaded transformer were used also for determining the magnetizing inductance  $L_m$  of the transformer. The measurement and calculation results are given in Table 3. The calculations were made after simplifying the waveform of the current  $i_1$  according to Fig. 11, using relationship (14) for  $T/2 = 5 \mu\text{s}$ .

#### Leakage inductance

The resultant leakage inductance  $L_\sigma = L_{\sigma 1} + L'_{\sigma 2}$  was determined from the analysis of the waveforms of the current  $i_1$  and the voltage  $u_1$  of the primary winding with the short-circuited secondary winding of the transformer (Fig. 12).

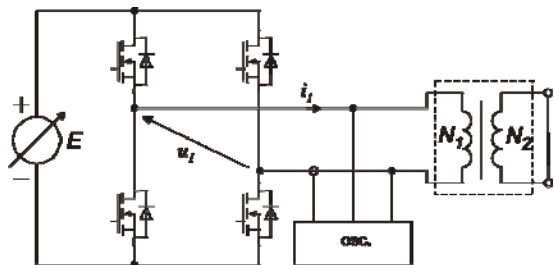


Fig. 12. A schematic diagram of the system for testing the short circuit transformer

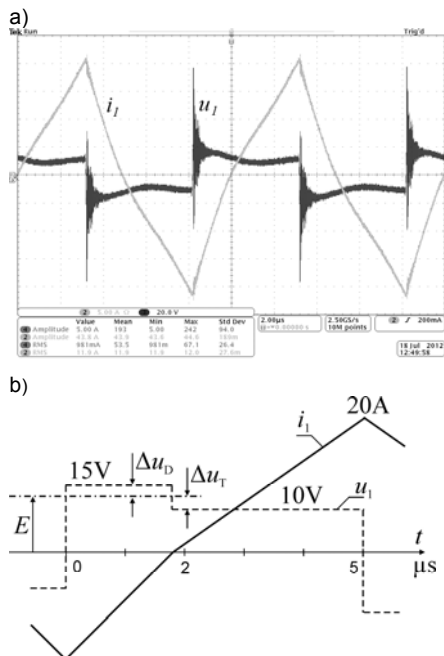


Fig. 13. Waveforms of the primary winding voltage and current of the short-circuited transformer (a) and the simplified waveforms of these quantities (b); 20 V/div; 5 A/div; 2 $\mu\text{s}$ /div

In this case, the measurements were taken at small values of the voltage  $E$  and at a current close to the rated current ( $I_{IRMS} \approx 10 \text{ A}$ ). Figure 13 shows example waveforms of the current  $i_1$  and the voltage  $u_1$ , along with the

approximated simplified waveforms of those quantities plotted on their basis.

Due to the large short-circuit current values and the large values of backward diode voltage drops  $\Delta u_D$  and transistor voltage drops  $\Delta u_T$ , the waveform of the voltage  $u_1$  exhibits distinct changes in levels, depending on whether the anti - parallel diodes or the transistors of the inverter's semiconductor switches conduct. Because of the inductive behaviour of the short-circuited transformer, in each voltage half-period, the anti - parallel diodes conduct first. Based on the simplified waveforms, for each recorded oscillogram, the voltage  $U_m$ , the peak current value  $I_{Im}$  and times  $\Delta t$  were determined, and then, using relationship (20), also the leakage inductance  $L_\sigma$  was determined. It was assumed, at the same time, the time constant  $L_\sigma/R_\sigma$  is many times greater than the voltage and the winding current period. The calculations considered the diode and transistor voltage drops, so the quantity  $U_m$  occurring in formula (20) was equal to  $E + \Delta u_D$  i  $E - \Delta u_T$ . The obtained measurement and calculation results, including the average value of  $L_{\sigma(AV)}$ , are given in Table 4.

Table 4. Measurements and calculations of the leakage inductance

$U_m$	$I_{Im}$	$\Delta t$	$L_m$	$L_{m(AV)}$
V	A	$\mu\text{s}$	$\mu\text{H}$	$\mu\text{H}$
3.50	7.82	3.0	1.33	1.41
5.20	7.80	2.0	1.33	
7.35	12.80	3.0	1.57	
10.0	15.0	2.0	1.33	
10.0	20.3	3.10	1.50	
15.0	20.5	1.92	1.40	

#### Winding resistances

In the case of the high-voltage winding for  $f = 100 \text{ kHz}$ , the characteristic values necessary for the calculation of the resistance increase coefficient and the resistance  $R_{\sigma 1}$ , at a temperature of  $20 \text{ }^\circ\text{C}$ , are equal to:  $y = 0.227 \text{ mm}$ ,  $m_{s2} = m_{s4} = 5.5$  and  $R_{d1} = 15 \text{ m}\Omega$ . For the calculation of the secondary winding resistance  $R_{\sigma 2}$ , it should be assumed that  $y = 2.27$ ,  $m_{s1} = m_{s3} = m_{s5} = 2$  and  $R_{d2} = 0.20 \text{ m}\Omega$  (Table 1). As a result of the calculations made based formula (21) or using nomograms provided in the literature (e.g. [3]), the following values were obtained:  $R_{\sigma 1} = 15.12 \text{ m}\Omega$  and  $R_{\sigma 2} = 1.4 \text{ m}\Omega$ .

Formula (21) is valid only for sinusoidal currents. In the deformed current waveforms of high-frequency transformers operating in power electronic equipment, in addition to the basic harmonic, higher harmonics of odd orders also occur. When conducting tests using the transformer circuit model, for the current harmonic components, the winding resistances for the frequencies 300 kHz, 500 kHz,... must be taken into account. This is especially important when determining the winding power losses. Due to the variations in skin-effect depth, with the increase in the frequency of the current harmonic components, the resistance increase coefficients takes on greater values (Fig. 14).

The graphs in Fig. 14 were plotted assuming the winding temperature at  $20 \text{ }^\circ\text{C}$ . When performing electrothermal modelling of a transformer, thermal variations in the electric conduction of copper, which cause changes in the direct current winding resistances  $R_{d1}$  and  $R_{d2}$ , and the variations in skin-effect depth, must be taken into account. These variations partially compensate for one another, which is clearly visible for the secondary winding, whose resistance at the frequency of 100 kHz decreases with increasing temperature. The relative winding resistances  $r_{\sigma 1}$  and  $r_{\sigma 2}$ , being the ratio of the winding resistances  $R_{\sigma 1(T)}$  and  $R_{\sigma 2(T)}$  of the transformer at  $T_T$  to the

winding resistances  $R_{\sigma 1}$  and  $R_{\sigma 2}$  at 20 °C, as a function of temperature, are illustrated in Fig. 15.

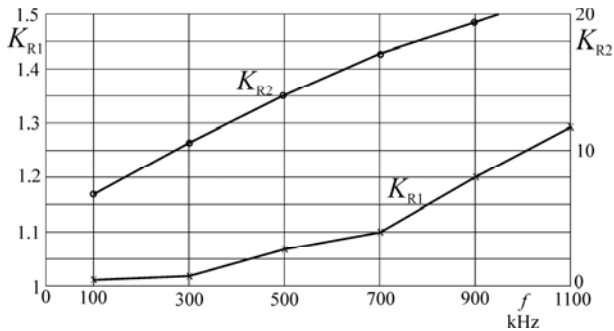


Fig. 14. Variations in the winding resistance increase coefficients of the transformer under consideration as a function of frequency

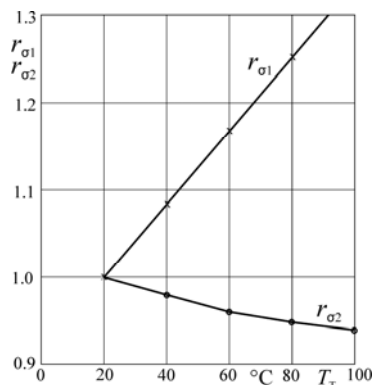


Fig.15. Relative variations in primary winding resistance  $r_{\sigma 1(T)}$  and secondary winding resistance  $r_{\sigma 2(T)}$  caused by temperature variations

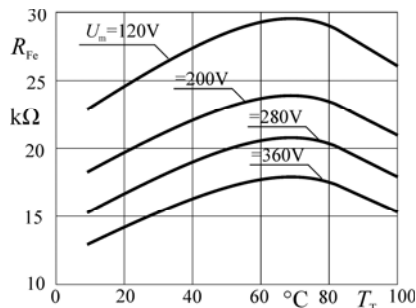


Fig. 16. Dependence of the resistance corresponding to the core power losses on the core temperature and the primary winding voltage

#### Resistance corresponding to core power losses

For the 3F3 ferrite core, Steinmetz's coefficients and the coefficients of the multinomial allowing for the temperature effect are:  $k = 0.25$ ;  $\alpha = 1.60$ ;  $\beta = 2.50$ ;  $c_0 = 1.26$ ;  $c_1 = 1,05 \times 10^{-2} \text{K}^{-1}$ ;  $c_2 = 0.79 \times 10^{-4} \text{K}^2$ .

It follows from relationships (16) – (18) that

$$(22) \quad R_{Fe} = \frac{U_m^{(2-\beta)}}{K_T (c_0 - c_1 T_T + c_2 T_T^2)}$$

where the constant  $K_T$  is expressed by the formula

$$(23) \quad K_T = \frac{8}{\pi^2} k f^{(\alpha-\beta)} (4N_1 S_{Fe})^{-\beta}$$

Figure 16 shows graphs illustrating the dependence of the resistance  $R_{Fe}$  on the core temperature  $T_T$  and the primary winding voltage  $U_m$ . The polynomial with the coefficients  $c_0$ ,  $c_1$  i  $c_2$  assumes a value equal to unity for a core temperature of approx. 30 °C and 100 °C. The minimum of this polynomial occurs at a temperature of approx. 70 °C.

#### Conclusions

The circuit models of transformers are very useful both in simulation and in the design of a wide range of power electronic converters, which contain high-frequency transformers in their main circuitry. The parameters of these models depend on the materials used for the construction of the core and the windings, their shape and geometrical dimensions, the relative positioning of the primary and secondary winding sections, as well as on other factors, including temperature. This makes their analytical description very difficult, and in many cases even impossible. Numerical modelling, though enabling the most accurate results to be obtained, is little useful in practice due to its time-consuming and complex nature.

The most reliable method of determining the transformer model parameters involves experimental measurements taken in conditions corresponding to the conditions prevailing during the transformer's operation in the system, in which it will be operated. This paper has presented a simple method for the experimental determination of the stray capacitance and leakage and magnetizing inductance on the basis of tests performed on a transformer operating without load and in a short - circuit state. A commercially available 5600 VA/ 100 kHz planar transformer was subjected to testing. The results of numerous experimental tests carried out at different supply voltages and different winding currents have shown satisfactory repeatability, which proves the correctness of the adopted testing methodology. To obtain the complete transformer circuit model, the remaining parameters, i.e. the winding resistances for alternating current and the resistance corresponding to the core power losses, have been calculated from Dowell's and Steinmetz's formulas. Considering the effect of temperature on the values of the resistance parameters of the developed model creates the possibility of using it in electrothermal modelling of the converter.

*This work was partially supported by the statutory activity of the Institute of Control and Industrial Electronics, Warsaw University of Technology.*

**Authors:** prof. dr hab. inż. Roman Barlik, dr inż. Piotr Grzejszczak, dr inż. Mariusz Zdanowski, Politechnika Warszawska, Instytut Sterowania i Elektroniki Przemysłowej, ul. Koszykowa 75, 00-662 Warszawa, E-mail: rbarlik@isep.pw.edu.pl; piotr.grzejszczak@ee.pw.edu.pl, mariusz.zdanowski@ee.pw.edu.pl

#### REFERENCES

- [1] Billings K. H., Switch mode power supply handbook, Mc Graw-Hill Publishing, New York, 1989
- [2] Pittini R., Zhang Z., Ouyang, Andersen M. A. E., Thomsen O. C., Analysis of planar E+I and ER+I transformers for low-voltage high-current DC/DC converters with focus on windings losses and leakage inductance, in Proc. IEEE 7<sup>th</sup> International Power Electronics and Motion Control Conference – ECCE Asia, Harbin, China, June 2-5, (2012), 488-493
- [3] Ouyang Z., Thomsen O. C., Andersen M. A. E., Optimal Design and Tradeoff Analysis of Planar Transformer in High – Power DC-DC Converters, IEEE Transactions on Industrial Electronics, 59 (2012), n.7, 2800-2810
- [4] Blaabjerg F., Chen Z., Kjaer B. S., Power electronics as efficient interface in dispersed power generation systems, IEEE Transactions on Power Electronics, 19 (2004), n.5, 1184-1194

- [5] Barlik R., Nowak M., Grzejszczak P., "Power transfer analysis in a single phase dual active bridge," *Bulletin of the Polish Academy of Sciences. Technical Sciences*, 61 (2013), n.4, 809-828
- [6] Yousefpoor N., Narwal A., Bhattacharya S., Control of DC-fault-resilient voltage source converter-based HVDC transmission system under DC fault operating condition, *IEEE Transactions on Industrial Electronics*, 62 (2015), n.6, 3683-3690
- [7] Ranstad P., Nee H.-P., On the distribution of AC and DC winding capacitances in high-frequency power transformers with rectifier loads, *IEEE Transactions on Industrial Electronics*, 58 (2011), n.5, 1789-1798
- [8] Citko T., *Energoelektronika. Układy wysokiej częstotliwości. Wydawnictwo Politechniki Białostockiej*, Białystok, 2007
- [9] Jałbrzykowski S., Citko T., Bridge configuration of class-E converters, *Archives of Electrical Engineering*, 52 (2003), n.2, 221-237
- [10] Kaczmarczyk Z., Poprawa właściwości energetycznych falowników klasy E przez maksymalizację wykorzystania tranzystora, *Zeszyty Naukowe Politechniki Śląskiej, Elektryka*, n. 200, Gliwice, 2007
- [11] Biela J., Kolar W. Using transformer parasitic for resonant converters – A review of the calculation of the stray capacitance of transformers, *IEEE Transactions on Industry Applications*, 44 (2008), n.1, 223 – 233
- [12] Górecki K., Zarębski J., Modeling nonisothermal characteristics of switch-mode voltage regulators, *IEEE Trans. Power Electronics*, 23 (2008), n.4, 1848-1858
- [13] Mućko J. Wybrane zastosowania technologiczne falowników rezonansowych, *Przegląd Elektrotechniczny (Electrical Review)*, 85 (2009), n.9, 273-278
- [14] Łyskawiński W., Field approach to power loss analysis of pulse transformer, *Archives of Electrical Engineering*, 56 (2007), n.2, 103-114.
- [15] Łyskawiński W., Polowa analiza wpływu konfiguracji uzwojeń na straty mocy w transformatorze impulsowym, *Przegląd Elektrotechniczny (Electrical Review)*, 86 (2010), n.4, 201-204
- [16] Han Y., Eberle W., Liu Y-F., A practical cooper loss measurement method for the planar transformer in high frequency switching converters, *IEEE Trans. Industrial Electronics*, 54 (2007), n.4, 2276-2287
- [17] Villar I., Viscarret U., Etxebarria-Otaudi I., Rufer A., Global loss evaluation methods for nonsinusoidally fed medium-frequency power transformers, *IEEE Transactions on Industrial Electronics*, 56 (2009), n.10, 4132-4140
- [18] Sippola M., Sepponen R. S., Accurate prediction of high – frequency power transformer losses and temperature rise, *IEEE Trans. Power Electronics*, 25 (2010), n.4, 850-862
- [19] Nowak M., Grzejszczak P., Zdanowski M., Barlik R., The thermovision method for windings power losses assessment of high frequency planar transformer, *Przegląd Elektrotechniczny (Electrical Review)*, 88 (2012), n.11, 60-63
- [20] Lu H. Y., Zhu J. G., Ramsden V. S., Hui S. Y. R., Measurement and modeling of stray capacitances in high frequency transformers, in *Proc. 30-th Annu. IEEE Power Electron. Spec. Conf. (PESC'99)*, Charleston, SC, June 27 – July 1 1999, 763-769
- [21] Lu H. Y., Zhu J. G., Hui S. Y. R., Experimental determination of stray capacitances in high frequency transformers, *IEEE Transactions on Industrial Electronics*, 18 (2003), n.5, 1105-1112
- [22] Dalessandro L., Cavalcante F. S., Kolar J. W., Self-capacitance of high-voltage transformers, *IEEE Trans. Power Electronics*, 22 (2007), n.5, 2081-2092,
- [23] Van den Bossche A., Valcher V. C., *Inductors and transformers in power electronics*, Taylor & Francis Group, Boca Raton, LLC, 2005
- [24] Dowell P. L., Effects of eddy currents in transformer windings, *IEE (UK)*, 113 (1966), n.8, 1387-1394

---

**Authors:** prof. dr hab. inż. Roman Barlik, dr inż. Piotr Grzejszczak, dr inż. Mariusz Zdanowski, Politechnika Warszawska, Instytut Sterowania i Elektroniki Przemysłowej, ul. Koszykowa 75, 00-662 Warszawa, E-mail: rbarlik@isep.pw.edu.pl; piotr.grzejszczak@ee.pw.edu.pl, mariusz.zdanowski@ee.pw.edu.pl